Single-Crystal ENDOR Study of a ^{57}Fe-Enriched Iron–Sulfur $[Fe_4S_4]^{3+}$ Cluster

G. Rius† and B. Lamotte*

Contribution from the Groupe de Spectroscopie des Complexes Polymétalliques et de Métalloprotéines (SCPM), Service de Physique, Département de Recherche Fondamentale, Centre d'Etudes Nucléaires de Grenoble (CEA), 85X, 38041 Grenoble Cedex, France.
Received June 20, 1988

Abstract: A new development of the method previously devised in order to study, by EPR, the paramagnetic states of the four iron–four sulfur clusters in single crystals is presented. In this paper, complete determination of the ^{57}Fe hyperfine tensors under high-resolution conditions has been obtained, thanks to the ENDOR study of ^{57}Fe-enriched single crystals of a synthetic model compound irradiated with γ-rays. This study, the first of its kind, has been made with the compound $(Et_4N)_2[Fe_4S_4(SCH_2Ph)_4]$, in the redox state $[Fe_4S_4]^{3+}$ of the cubane which corresponds to the oxidized state of the high-potential (HP) ferredoxins. The results are in good agreement with those of previous Mössbauer and ENDOR studies. They corroborate the model based on two pairs of coupled iron atoms: a mixed-valence pair and a ferric pair. But these results are much more precise, and they also provide new information, especially about the principal directions of the hyperfine tensors of the four ^{57}Fe atoms. Their analysis shows that the four tensors are all different and thus that the symmetry of the $[Fe_4S_4]^{3+}$ cubane is lower than could be expected on the grounds of previous results. However, since this new field is now just being opened, further results of this kind are clearly needed in order to interpret these tensors fully and to get new insights into the electronic structure and the spin density distribution in the paramagnetic states of these clusters.

I. Introduction

A great number of measurements, especially by Mössbauer, EPR, NMR, and magnetic susceptibility methods, have already been made on iron–sulfur proteins[1a-h] and also on their synthetic analogues.[2a-c] Phenomenologic models based on spin couplings of iron atoms in their high-spin states appear able to interpret rather satisfactorily the principal experimental features of these iron–sulfur clusters.[3a-c] Moreover, first principles calculations, based on the Xα method, seem able to reproduce and to interpret these results in a more fundamental way.[4a-d] However, we think that much further progress in the physical understanding of these structures could be obtained if more precise and more detailed observables than those obtained until now could be gained from new experiments.

The essential *limitation* of the current studies of iron–sulfur clusters, in the proteins as well as in their synthetic analogues, is due to the fact that they have always been conducted in *non-oriented systems*: frozen solutions or polycrystalline powders. Consequently, there is a double limitation. First, the data are incomplete. In EPR, for instance, the complete determination of the **g** or of the hyperfine tensors is impossible, and only the principal values of these tensors can be obtained. The second limitation is on resolution: the lines are broad and not well resolved. This is true even for electron-nuclear double resonance (ENDOR) which is the high-resolution double resonance method adjunct to EPR. For instance, the ENDOR ^{57}Fe studies of ferredoxins[5a-d] have been of great interest but, because of the disorder in the orientations of the clusters (and also of the distribution of their geometries), the ENDOR lines reported are quite broad, poorly structured, and difficult to extract from the proton ENDOR lines also present in the spectra. The most remarkable results of this kind have been obtained recently by ENDOR of the ^{57}Fe-enriched iron–molybdenum nitrogenase enzyme by Hoffman et al.[6] These authors have taken advantage of the large anisotropy of the effective **g** tensor of the $S = {}^3/_2$ state of the unknown cluster to obtain rather well-resolved "single-crystal-like" ENDOR spectra at extrema turning points of the EPR spectrum. Moreover, with the help of simulations of the ENDOR spectra, they were able to deduce approximate relative orientations of the hyperfine tensors of the ^{57}Fe atoms with respect to the axis of the effective **g** tensor. However, in their discussion, the authors of this fine piece of work pointed out the unavoidable uncertainties which are common to studies of polycrystalline and frozen solution samples. Although this difficulty is certainly inherent to protein studies, we want to show that for synthetic models it is possible to obtain, simultaneously, a much better resolution and a complete determination of the hyperfine tensors.

As is general in spectroscopy, *single-crystal studies* represent the only way to attain the highest resolution as well as the complete measurement of the anisotropic observables involved in the problem. Gloux et al. have previously begun such an approach for the EPR study of the $[Fe_4S_4]^+$ and $[Fe_4S_4]^{3+}$ paramagnetic states in single crystals of the synthetic cubanes.[7] The method is the following. Single crystals of the synthetic complex in its redox state $[Fe_4S_4]^{2+}$ are grown. Then, they are irradiated with γ-rays which create, in situ, both the "oxidized" species $[Fe_4S_4]^{3+}$ and the "reduced" species $[Fe_4S_4]^+$. The first species correspond to trapped holes and the second ones to trapped electrons. They are oriented and diluted at relatively low concentration in the crystal matrix composed of diamagnetic $[Fe_4S_4]^{2+}$ cubanes. Since the nuclear spins of ^{56}Fe and ^{32}S (the most abundant natural

† Also at the Université J. Fourier, Grenoble.

(1) (a) Orme-Johnson, W. H.; Sands, R. H. In *Iron-Sulfur Proteins*; Lovenberg, W., Ed.; Academic Press: New York, 1973; Vol. II, p 195. (b) Bearden, A. J.; Dunham, W. R. *Ibid.* p 239. (c) Phillips, W. D.; Poe, M. *Ibid.* p 255. (d) Palmer, G. *Ibid.* p 286. (e) Cammack, R.; Dickson, D. P. E.; Johnson, C. E. In *Iron-Sulfur Proteins*; Lovenberg, W., Ed.; Academic Press: New York, 1977; Vol. III, p 283. (f) Debrunner, P. G.; Münck, E.; Que, L.; Schulz, C. E. *Ibid.* p 381. (g) Orme-Johnson, W. H.; Orme-Johnson, N. R. In *Iron-Sulfur Proteins*; Spiro, T. G., Ed.; Wiley-Interscience: New York, 1982; Vol. IV p 67. (h) Münck, E. *Ibid.* p 147.

(2) (a) Holm, R. H.; Ibers, J. A. In *Iron-Sulfur Proteins*, Vol. III; Lovenberg, W., Ed.; Academic Press, New York, 1977; p 205. (b) DeBrunner, P. G.; Münck, E.; Que, K.; Schulz, C. E. *Ibid.* p 381. (c) Berg, J. M.; Holm, R. H. In *Iron-Sulfur Proteins*; Spiro, T. G., Ed.; Wiley-Interscience: New York, 1982; Vol. 4, p 1.

(3) (a) Papaefthymiou, V.; Girerd, J.-J.; Moura, I.; Moura, J. J. G.; Münck, E. *J. Am. Chem. Soc.* **1987**, *109*, 4703. (b) Noodleman, L.; Case, D. A.; Aizman, A. *Ibid.* **1988**, *110*, 1001. (c) Noodleman, L. *Inorg. Chem.* **1988**, *27*, 3677.

(4) (a) Norman, J. G.; Ryan, P. B.; Noodleman, L. *J. Am. Chem. Soc.* **1980**, *102*, 4279. (b) Aizman, A.; Case, D. A. *Ibid.* **1982**, *104*, 3269. (c) Noodleman, L.; Baerends, E. J. *Ibid.* **1984**, *106*, 2316. (d) Noodleman, L.; Norman, J. G.; Osborne, J. H.; Aizman, A.; Case, D. A. *Ibid.* **1985**, *107*, 3418.

(5) (a) Fritz, J.; Anderson, R.; Fee, J.; Palmer, G.; Sands, R. H.; Tsibris, J. C. M.; Gunsalus, I. C.; Orme-Johnson, W. H.; Beinert, H. *Biochim. Biophys. Acta* **1971**, *253*, 110. (b) Mukai, K.; Kimura, T.; Helbert, J.; Kevan, L. *Ibid.* **1973**, *295*, 49. (c) Anderson, R. E.; Dunham, W. R.; Sands, R. H.; Bearden, A. J.; Crespi, H. L. *Ibid.* **1975**, *408*, 306. (d) Anderson, R. E.; Anger, G.; Petersson, L.; Ehrenberg, A.; Cammack, R.; Hall, D. O.; Mullinger, R.; Rao, K. K. *Ibid.* **1975**, *376*, 63.

(6) True, A. E.; Nelson, M. J.; Venters, R. A.; Orme-Johnson, W. H.; Hoffman, B. M. *J. Am. Chem. Soc.*, **1988**, *110*, 1935.

(7) Gloux, J.; Gloux, P.; Lamotte, B.; Rius, G. *Phys. Rev. Lett.* **1985**, *54*, 599.

0002-7863/89/1511-2464$01.50/0

isotopes) are zero, these investigations have been restricted to the study of the **g** tensors until now. But hyperfine tensors constitute very relevant observables of the electronic and magnetic structures since they give the potential to map in a detailed way the spin density distribution in these clusters. Therefore, it would be very interesting to measure them precisely and completely.

The present article represents the first step in this new direction. It shows that the use of isotopically enriched single crystals combined with the use of the ENDOR technique allows the complete determination of the hyperfine tensors with a resolution between one and two orders of magnitude better than the resolution that EPR or Mössbauer methods have given in previous studies. Indeed, these results clearly show that it is only by using single crystals that we gain the inherent higher resolution of ENDOR with respect to EPR and Mössbauer.

This study is devoted to the investigation of a $[Fe_4S_4]^{3+}$ cluster representing the synthetic analogue of the oxidized state of the active site of the high-potential (HP) ferredoxins. It has been made in the $(Et_4N)_2[Fe_4S_4(SCH_2Ph)_4]$ (**1**) compound. The results presented here will be compared with those of EPR,[8] ENDOR,[5d] and Mössbauer[9] studies of the $[Fe_4S_4]^{3+}$ state in HP ferredoxins and also with the recently published study of the first synthetic complex prepared in the $[Fe_4S_4]^{3+}$ state.[10a,b]

II. Experimental Section

1. Preparation of $(Et_4N)_2[Fe_4S_4(SCH_2Ph)]$ Enriched with ^{57}Fe. Iron chloride, $FeCl_2 \cdot 4H_2O$, enriched with ^{57}Fe was prepared under an argon atmosphere from 78 mg of ^{57}Fe (isotopic purity ≥95%) purchased from the Service des Isotopes Stables C.E.N., Saclay CEA, France, and from ultrapure hydrochloric acid Normatom from Prolabo. This enriched iron chloride was then used to prepare $(Et_4N)_2[Fe_4S_4(S\text{-}t\text{-}Bu)_4]$ enriched with ^{57}Fe by following the synthesis procedure of Garner et al.[11] The final compound was obtained by ligand exchange with benzyl mercaptan in acetonitrile. The different steps of the preparation of the complex were conducted in a glove box under an argon atmosphere (1 ppm of O_2) in glassware especially made for the use of small quantities. We could obtain 275 mg of $(Et_4N)_2[Fe_4S_4(SCH_2Ph)_4]$ enriched with ^{57}Fe, corresponding to a yield of 76%.

The crystallographic structure of this compound has been published by Averill et al.[12] It crystallizes in the monoclinic space group $P2_1/c$ with $Z = 4$. Two magnetically inequivalent sites of the clusters are present in the unit cell, which become equivalent in ESR experiments when the static magnetic field is in the glide plane ac or when it lies along the screw axis $\vec{b}$. The site whose coordinates are reported in ref 12 will be called site 1 or cluster 1 in the following. The $[Fe_4S_4]^{2+}$ cores of these clusters have the shapes of distorted cubes with iron and sulfur atoms occupying alternate vertices. They exhibit an approximate, compressed D_{2d} distortion from cubic symmetry where the idealized $\bar{4}$ axis of the distortion is perpendicular to the two Fe_1–Fe_2 and Fe_3–Fe_4 bonds directions.

Single crystals of approximate dimensions 5 × 2 × 1 mm have been obtained by a transport method in a solution of the compound in acetonitrile. Their greatest dimension corresponds to the $\vec{a}$ axis. Their glide plane ac can be obtained by cleavage. These single crystals have been irradiated with a ^{60}Co source, under argon atmosphere and at room temperature, to a dose of about 10 Mrads.

2. EPR and ENDOR Methodology. The EPR spectra were recorded either on a Varian E 109 spectrometer or on a Bruker ER 200 D-SRC spectrometer, both equipped with an Oxford Instruments ESR-9 continuous-flow helium cryostat.

The ENDOR experiments were performed on the Bruker spectrometer with the Varian E 1700 broad-band ENDOR accessory and a 100-W ENI 3100 L broad-band power amplifier. The ENDOR spectra were detected with amplitude modulation of the radio frequency (generally at 3.25 kHz), without magnetic field modulation. For double-ENDOR experiments, a generator/sweeper Hewlett Packard Model 8601 A was used.

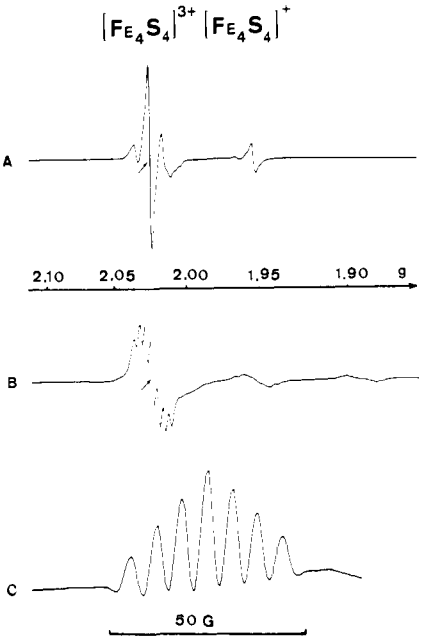

Figure 1. EPR spectra (9.23 GHz) of γ-irradiated single crystals of $(NEt_4)_2[Fe_4S_4(SCH_2Ph)_4]$ with the static magnetic field along the $\vec{c}^*$ axis of the crystal: (A) single crystal synthesized from natural abundance iron, observed at 17 K, microwave power = 0.5 mW, magnetic field modulation = 4 G; (B) single crystal synthesized from ^{57}Fe, observed at 10 K, microwave power = 0.2 mW, magnetic field modulation = 4 G; (C) second derivative of the spectrum of the $[^{57}Fe_4S_4]^{3+}$ center labeled by an arrow in (B), temp 15 K, microwave power = 5 mW, magnetic field modulation = 4 G.

Table I. **g** Tensor of the $[Fe_4S_4]^{3+}$ Center Studied in This Work, and Comparison of the Direction Cosines of Its Principal Directions in the $\vec{a}$, $\vec{b}$, $\vec{c}^*$ Reference Frame with the Directions Related to Iron–Iron Bonds in Site 1 of the $[Fe_4S_4]^{2+}$ Cluster[12]

	principal directions direction cosines with respect to		
principal values	$\vec{a}$	$\vec{b}$	$\vec{c}^*$
$g_1 = 2.066$	0.051	0.971	−0.234
$g_2 = 2.025$	0.744	0.119	0.658
$g_3 = 2.014$	0.666	−0.208	−0.716
$g_{av} = 2.035$			
$\overrightarrow{Fe_1Fe_2} \times \overrightarrow{Fe_3Fe_4}$	−0.131	−0.988	0.081
$\overrightarrow{Fe_1Fe_2}$	−0.744	0.044	−0.667
$\overrightarrow{Fe_3Fe_4}$	0.653	−0.147	−0.743

III. Experimental Results

1. EPR Study of the Natural Abundance and ^{57}Fe-Enriched Crystals. Comparison of two γ-irradiated single crystals of compound **1**, the first with natural abundance of iron and the second being enriched with ^{57}Fe, is shown in Figure 1a,b. Since these spectra are taken along the $\vec{c}^* = \vec{a} \times \vec{b}$ axis, the two magnetic sites in the crystal are equivalent, and each line in the spectrum corresponds to a particular paramagnetic center.

Following the analysis developed in previous papers,[7,13] the angular dependence of these anisotropic lines and their temperature behavior allow us to class them into two groups. In the first group, the lines are centered around $g = 2.02$ in the spectra of Figure 1a,b and have average g values greater than 2. They correspond to the oxidized clusters $[Fe_4S_4]^{3+}$. In the second group, the lines, centered around $g = 1.96$, have average g values less than 2 and correspond to the reduced clusters $[Fe_4S_4]^{+}$. (Note that complete EPR studies of these paramagnetic species will appear in a later paper.[14]

(8) (a) Antanaitis, B. C.; Moss, T. H. *Biochim. Biophys. Acta* **1975**, *405*, 262. (b) Beinert, H.; Thomson, A. J. *Arch. Biochem. Biophys.* **1983**, *222*, 333.
(9) Middleton, P.; Dickson, D. P. E.; Johnson, C. E.; Rush, J. D. *Eur. J. Biochem.* **1980**, *104*, 289.
(10) (a) O'Sullivan, T.; Millar, M. M. *J. Am. Chem. Soc.* **1985**, *107*, 4096. (b) Papaefthymiou, V.; Millar, M. M.; Münck, E. *Inorg. Chem.* **1986**, *25*, 3010.
(11) Christou, G.; Garner, C. D. *J. Chem. Soc., Dalton Trans.* **1979**, 1093.
(12) Averill, B. A.; Herskovitz, T.; Holm, R. H.; Ibers, J. A. *J. Am. Chem. Soc.* **1973**, *95*, 3524.
(13) (a) Gloux, J.; Gloux, P.; Hendriks, H.; Rius, G. *J. Am. Chem. Soc.* **1987**, *109*, 3220. (b) Gloux, J.; Gloux, P. 19th International Conference on ESR of Inorganic Radicals and Metal Ions in Inorganic and Biological Systems, York, England, April 1987.

The present study is dedicated to the paramagnetic center corresponding to an electronic spin $S = {}^1/_2$ whose spectrum, indicated by an arrow in Figure 1a, appears as the most intense in the group of lines labeled $[Fe_4S_4]^{3+}$. This spectrum is obtained in the best conditions around 10 K with a microwave power of 0.1 mW. It is very easily saturated at 4.2 K and it broadens out at about 40 K.

In order to characterize this center, its **g** tensor has been determined from the angular dependence of its ESR lines in the three orthogonal planes: *ab*, *bc**, and *c***a* and, in addition, in a fourth plane in order to lift the remaining ambiguities in the determination of the tensor. Its **g** tensor in the $\vec{a}$, $\vec{b}$, $\vec{c}^*$ reference frame is presented in Table I. This table also contains for comparison the direction cosines of the $\overrightarrow{Fe_1Fe_2} \times \overrightarrow{Fe_2Fe_4}$, $\overrightarrow{Fe_1Fe_2}$, and $\overrightarrow{Fe_3Fe_4}$ directions of cluster 1. The comparison shows that there is a strong correlation between the principal directions of the **g** tensor and the latter three directions. We find that the $\vec{g}_3$ axis is very close to the $\overrightarrow{Fe_3Fe_4}$ direction (their mutual angle being 4°). This was already observed in $(Et_4N)_2[Fe_4S_4(S\text{-}t\text{-}Bu)_4]$.[13b] $\vec{g}_2$ is perpendicular to this direction and the largest value, g_1, has its axis which is nearly perpendicular to the $\overrightarrow{Fe_3Fe_4}$ and $\overrightarrow{Fe_1Fe_2}$ directions. This means that the principal direction $\vec{g}_1$ is very close to the approximate $\bar{4}$ axis of the $[Fe_4S_4]^{2+}$ cubane. The latter characteristic has already been found in the previous study of the single crystals of $(Bu_4N)_2[Fe_4S_4(SPh)_4]$.[7,13] These results emphasize that the Fe–Fe bond directions must play a major role in the description of these paramagnetic states.

We note that, until now, the identification of the paramagnetic species studied here as being $[Fe_4S_4]^{3+}$ (as well as the assignments of all the other EPR lines shown in Figure 1a) relies only on the comparison with the spectroscopic data for previously identified species in proteins and in model compounds.[7,13] The study of the ^{57}Fe-enriched samples described below will confirm definitively these assignments.

Examination of the spectrum of Figure 1b, corresponding to the ^{57}Fe-enriched crystal, shows that all the EPR lines assigned in Figure 1a to $[Fe_4S_4]^{3+}$ and $[Fe_4S_4]^{+}$ centers are now broadened and in some cases exhibit more or less well-resolved hyperfine interactions with ^{57}Fe nuclei ($I = {}^1/_2$). This result constitutes definitive proof that γ-irradiation creates only paramagnetic species at the iron–sulfur cubane itself, not free radicals in the thiolate ligands or in the tetraethylammonium counterions.

The $[Fe_4S_4]^{3+}$ center studied here exhibits a well-resolved hyperfine pattern of interactions with ^{57}Fe. By detecting its second derivative, we can improve the resolution of the spectrum; conditions of temperature and microwave power can also be chosen in order to minimize the spectra of the paramagnetic centers which overlap with it. Figure 1c presents the corresponding EPR spectrum showing that the ^{57}Fe hyperfine interaction gives rise to seven lines having relative intensities close to 1–2–3–4–3–2–1. Such a pattern immediately shows that there are hyperfine couplings with two pairs of equivalent (or nearly equivalent) ^{57}Fe atoms, the hyperfine interaction for the atoms of one pair being close to twice the hyperfine interaction for the atoms of the other pair (about 13 G for the first pair and 6.5 G for the second pair, along the $\vec{c}^*$ axis). We can observe that this preliminary results is in good agreement with the Mössbauer hyperfine parameters reported for HP proteins[9] and for the monocationic synthetic compound $(Bu_4N)[Fe_4S_4(S\text{-}2,4,6\text{-}i\text{-}Pr_3C_6H_2)_4]$.[10b] Nevertheless, completely satisfactory computer reconstitutions using the above hyperfine couplings (either with Gaussian or Lorentzian line shapes) cannot be obtained. Small differences are always observed in the relative intensities of the lines and in their separations. Relatively, the best fits are obtained by allowing the ^{57}Fe hyperfine couplings to be somewhat *different* in each of the two pairs. Moreover, if the orientation of the crystal is changed from the orientation shown in Figure 1, either in the *bc** or in the *c***a* planes, there are smooth variations of the hyperfine splittings which indicate that these hyperfine interactions are not very anisotropic.

(14) Gloux, J.; Gloux, P., to be published.

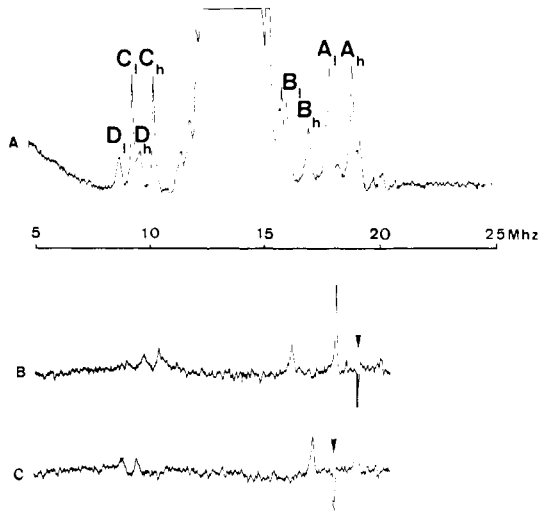

Figure 2. ENDOR and double-ENDOR spectra of a γ-irradiated single crystal of $(NEt_4)_2[Fe_4S_4(SCH_2Ph)_4]$ synthetized from ^{57}Fe. The static magnetic field is along the $\vec{c}^*$ axis of the crystal. (A) ENDOR spectrum at 4 K; microwave power = 1.45 mW; radio-frequency power = 100 W; amplitude modulation frequency = 1.56 kHz; scan time = 4 min; time constant = 0.3 s. The four doublets of ^{57}Fe ENDOR lines are labeled on the spectrum. They correspond to the four ^{57}Fe hyperfine tensors reported in Table II. In each doublet, the subscript h corresponds to the *higher* frequency ENDOR transition and the subscript l to the *lower* frequency ENDOR transition. The other ENDOR lines are due to protons except for the small lines in the range of frequency of the two A lines and above. The latter correspond to ^{57}Fe ENDOR lines due to the other varieties of $[Fe_4S_4]^{3+}$ centers mentioned in Figure 1, whose EPR spectra overlap with the EPR spectrum of the main species studied here. (B) Double-ENDOR spectrum at 4 K with radio-frequency irradiation of the A_l ENDOR line; microwave power = 0.72 mW; fixed radio-frequency power = 50 W; swept radio-frequency power = 50 W; amplitude modulation frequency = 1.56 kHz; scan time = 4 min; time constant = 0.6 s. (C) Double-ENDOR spectrum at 4 K with radio-frequency irradiation of the A_h line. The experimental conditions are similar to those used for the B spectrum.

However, progressive loss of resolution is observed when one gets away from this axis. This indicates that, in spite of the well-resolved spectrum shown in Figure 1c, detailed information about hyperfine interactions cannot be obtained by EPR alone. As we will see in the continuation of this text, it is only by relying on the much higher resolution of ENDOR that this information can be obtained.

2. ENDOR Study of the ^{57}Fe Hyperfine Interactions. A typical ENDOR spectrum, obtained with the magnetic field oriented along the $\vec{c}^*$ axis of the crystal, is shown in Figure 2a. This spectrum corresponds to the superposition of proton and ^{57}Fe ENDOR lines. We can distinguish the following.

(1) A strong and broad clump of lines centered at $\nu_H = 13.73$ MHz (which corresponds to the proton nuclear Zeeman frequency in the static magnetic field H_0 of this experiment) and which corresponds to weakly coupled protons pertaining to the benzyl groups liganded to the $[Fe_4S_4]^{3+}$ center or to the vicinal $(Et_4N)^+$ cations.

(2) A set of eight lines which can be associated in two groups of two doublets, each doublet being labeled A,B and C,D. As these lines do not exist for the nonenriched samples, they must be identified with ^{57}Fe. Moreover, the line separation in the four doublets is nearly equal to twice the nuclear Zeeman frequency of ^{57}Fe ($\nu_{Fe} = 0.89$ MHz) in the applied magnetic field. The doublets A and B correspond to hyperfine coupling with two ^{57}Fe atoms more strongly coupled and the doublets C and D to hyperfine coupling with two other iron nuclei, the later being half the former.

Thus, the ENDOR spectra confirm much more precisely the results of the above EPR study. The widths of the ^{57}Fe ENDOR lines are not all the same, but they are always between 100 to 200 kHz. Compared to the absolute value of the hyperfine couplings they lead to a measurement resolution *better than 100*. By

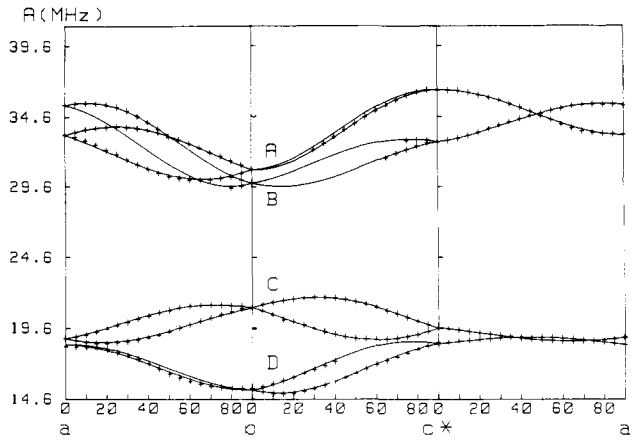

Figure 3. Angular dependences of the ^{57}Fe hyperfine couplings deduced from the ENDOR experiment in the three orthonormal planes *ab*, *bc**, and *c*a*. These hyperfine couplings are labeled A, B, C, D by reference to the ENDOR lines of Figure 2. They correspond to the four ^{57}Fe hyperfine tensors of the same names presented in Table II. The crosses (+) represent experimental points and the continuous curves represent computer fits.

comparison, the resolution of ESR and Mössbauer measurements on these systems is *between one and two orders of magnitude lower*.

The hyperfine interaction tensors of the four iron nuclei have been determined by studying (successively for the EPR lines belonging to the two inequivalent magnetic sites of the cluster) the angular dependences of the corresponding ENDOR lines in the three orthonormal planes *ab*, *bc**, and *c*a*. The spin-Hamiltonian corresponding to the ENDOR spectra is composed of three terms: the electronic Zeeman term $\mathcal{H}_{ZE}$, the nuclear Zeeman term relative to the ^{57}Fe nuclei $\mathcal{H}_{ZN}$, and the ^{57}Fe hyperfine interaction terms $\mathcal{H}_{HF}$. Since $\mathcal{H}_{ZE} \gg \mathcal{H}_{HF} \gg \mathcal{H}_{ZN}$, the two lines in each doublet correspond to the two ENDOR transitions $\Delta m_I = \pm 1$ associated with $M_s = {}^1/_2$ or $M_s = -{}^1/_2$. Their frequencies are given by $(a_{Fe} \pm (\nu_{Fe} + \epsilon))$, where a_{Fe} is the hyperfine interaction of a given nucleus and $\epsilon \sim (a_{Fe})^2/4H_0$ is the second-order term. The higher frequency lines and the lower frequency lines are labeled A_h, B_h, C_h, D_h and A_l, B_l, C_l, D_l, respectively. Thus, for any orientation, the hyperfine interactions correspond to the average of the frequencies of the two lines in each doublet. Their values are shown in Figure 3 as a function of the orientation of the static magnetic field in the three orthogonal planes *ab*, *bc**, and *c*a*. After computer fitting of these curves and tensor diagonalizations, we deduce the four iron hyperfine tensors which are reported in Table II (for fitting procedures, see, for example, ref 15).

Perfect orientation of the crystal in the three planes is difficult to obtain, and, in particular, the matching of the line positions along a common axis at the junction of two planes is not completely perfect; this introduces some inaccuracy in the determination of the hyperfine tensors. Since the anisotropy of the hyperfine interactions is small, this inaccuracy affects mainly the principal directions. This explains also why the hyperfine interactions (isotropic plus anisotropic) have been given with a precision of three significant figures.

For comparison, the ^{57}Fe hyperfine parameters deduced from Mössbauer studies in respectively, the monocationic model compound:

$$(Bu_4N)_2[Fe_4S_4(S\text{-}2,4,6\text{-}i\text{-}Pr_3C_6H_2)_4]^{10b}$$

and in the oxidized *C. vinosum* HP protein,[9a] are reported in Table III. It is important to note that, by contrast with our measurements, the spatial orientations of the hyperfine tensors relative to the cluster are not determined in these Mössbauer experiments; for each iron site, the orientation of the hyperfine tensor is referred only to the principal directions of the electric field gradient tensor.

(15) Gordy, W. *Theory and Applications of E.S.R.* (*Techniques of Chemistry*, Vol. 15); West, W., Ed.; Wiley: New York, 1980.

Table II. Principal Values and Principal Directions of the Four ^{57}Fe Hyperfine Tensors **A**, **B**, C, **D** of the $[Fe_4S_4]^{3+}$ Center Deduced from the ENDOR Experiment[a]

tensors of ^{57}Fe	principal values (in MHz)			principal directions: direction cosines with respect to		
	total	isotropic	anisotropic	$\vec{a}$	$\vec{b}$	$\vec{c}^*$
A	$\mathbf{A}_1 = -36.5$		−3.0	0.010	−0.029	0.999
	$\mathbf{A}_2 = -33.9$	−33.5	−0.4	−0.911	0.412	0.021
	$\mathbf{A}_3 = -30.1$		+3.4	−0.412	−0.911	−0.022
B	$\mathbf{B}_1 = -35.7$		−3.0	0.959	−0.194	−0.208
	$\mathbf{B}_2 = -32.8$	−32.7	−0.1	−0.240	−0.165	−0.956
	$\mathbf{B}_3 = -29.5$		+3.2	−0.151	−0.967	0.205
C	$C_1 = 21.8$		+2.0	0.148	−0.869	−0.472
	$C_2 = 19.6$	19.8	−0.2	−0.703	0.243	−0.669
	$C_3 = 18$		−1.8	0.695	0.431	−0.575
D	$\mathbf{D}_1 = 19.0$		+1.6	0.625	0.135	−0.769
	$\mathbf{D}_2 = 18.1$	17.4	+0.7	−0.778	0.194	−0.598
	$\mathbf{D}_3 = 15.0$		−2.4	−0.068	−0.972	−0.226

[a] Note that the sign of the principal values of the tensor **A** (or **B**) is taken from previous Mössbauer experiments,[10b] while the signs of the other tensors are deduced from our double-ENDOR experiment.

Table III. Hyperfine Parameters of $(Fe_4S_4)^{3+}$ for $(Bu_4N)[Fe_4S_4(S\text{-}2,4,6\text{-}i\text{-}Pr_3C_6H_2)_4]$ in Polycrystalline Form and in Frozen Toluene Solution[10b] and for *C. vinosum* Oxidized HP Protein[9] as Deduced from Mössbauer Experiments[a]

	A_x (MHz)	A_y (MHz)	A_z (MHz)	A_{av} (MHz)
Polycrystalline $(Bu_4N)[Fe_4S_4(S\text{-}2,4,6\text{-}i\text{-}Pr_3C_6H_2)_4]$				
α pair ($Fe^{2.5+}$–$Fe^{2.5+}$)	−28.8	−32.5	−34.3	−32
β pair (Fe^{3+}–Fe^{3+})	+22.6	+20.6	+17.4	+20.2
$(Bu_4N)[Fe_4S_4(S\text{-}2,4,6\text{-}i\text{-}Pr_3C_6H_2)_4]$ in Frozen Toluene Solution				
α pair ($Fe^{2.5+}$–$Fe^{2.5+}$)	−28.1	−32.2	−32.9	−31.1
β pair (Fe^{3+}–Fe^{3+})	+21.9	+20.6	+18.5	+20.3
C. vinosum Oxidized HP Protein				
α pair ($Fe^{2.5+}$–$Fe^{2.5+}$)	−28.2	−30.6	−32.5	−30.4
β pair (Fe^{3+}–Fe^{3+})	19.2	22.4	19.3	20.3

[a] These parameters are referred to the principal directions of the electric field gradient tensor.

A last point in this comparison concerns the *signs* of the different ^{57}Fe hyperfine tensors. For this problem, the Mössbauer technique is superior because it is easy to deduce the signs from the displacements of the magnetic Mössbauer lines as a function of the applied static magnetic field. By contrast, the ENDOR experiments reported above only measure the energies of the transitions between the different nuclear spin states; thus they cannot give the signs.

For this reason, we have done supplementary double-ENDOR experiments for one selected orientation (the $\vec{c}^*$ axis). This technique makes it possible to determine the *relative signs* of the hyperfine tensors of the four iron atoms. In this method, the relative signs of two different hyperfine couplings can be determined by using two simultaneous radio-frequency fields. The principle is as follows:[16] if we consider two different nuclei of spin ${}^1/_2$ (here two ^{57}Fe), the higher frequency ENDOR transitions for each nucleus (and also the lower frequency transitions for each) correspond to nuclear spin transitions within the same set of nuclear sublevels, associated with $m_s = +{}^1/_2$ or $m_s = -{}^1/_2$, *if the hyperfine couplings of these two nuclei have the same sign*. Conversely, they must correspond to nuclear spin transitions within different nuclear subsets (one in the subset of $m_s = +{}^1/_2$ and the other in the subset of $m_s = -{}^1/_2$) if the hyperfine couplings of these two nuclei have opposite signs. *Moreover*, it is generally found that two simultaneous ENDOR transitions *enhance* each other's intensity if they occur in the *two different nuclear subsets* while, conversely, there is a reduction of their intensity or no effect at all if they both occur in the *same subset*. It is this difference of behavior which is used to determine the relative signs of the

(16) Cook, R. J.; Whiffen, D. H. *Proc. Phys. Soc.* **1964**, *84*, 845.

hyperfine couplings of the four iron atoms corresponding to the four tensors *A*, *B*, *C*, *D* of Table II.

Figure 2b shows the double-ENDOR spectrum obtained when the static magnetic field is along the $\vec{c}^*$ axis and when the ENDOR line A_h is irradiated with the first (amplitude modulated) fixed radio frequency (indicated by the arrow). In these conditions the baseline of the spectrum of Figure 2b corresponds to the level of the peak of this ENDOR line A_h. We see that the intensity of this line is increased when the second radio-frequency field is swept through the ENDOR lines A_l, B_l, C_h, and D_h. This means that the four nuclear transitions corresponding to these last lines and the nuclear transition corresponding to the A_h line do not belong to the same subset of electron spin states. The experiment of Figure 2c confirms this result; when A_l is irradiated, the increase of intensity now corresponds to the lines A_h, B_h, C_l, and D_l.

The net result of this experiment is that the tensors A and B of the first two ^{57}Fe have the *same* signs; those of the last two, C and D, also have the *same* signs, but their signs are *opposite* to those of A and B. This result is in perfect agreement with the signs determined by Mössbauer experiments and which are reported in Table III. Moreover, this experiment is interesting for another reason. In effect, the difference in intensities and widths of different ^{57}Fe ENDOR lines in Figure 2a (for instance, between the lines of the C and D doublets) could cause some doubt due to the fact that they all belong to the $[Fe_4S_4]^{3+}$ center studied here. This is because, as seen in Figure 1a, EPR lines of other varieties of $(Fe_4S_4)^{3+}$ species lie close to the ESR line of this center. The interest of this double-ENDOR experiment is that it proves that the four ENDOR doublets A, B, C, D correspond to the four iron atoms of the paramagnetic center studied here.

IV. Discussion of the Results

The first remark is that our results in Table II and those contained in Table III compare so well for the different parameters common to the two tables that there cannot be any doubt that we are studying the same species and hence that our method is fundamentally valid.

As in previous studies, our results indicate the existence of two different pairs of iron atoms. Thus, the proposed model[3c,9,10] of the $[Fe_4S_4]^{3+}$ state made up of two coupled pairs of iron atoms—an α pair of two mixed-valence $Fe^{2.5+}$–$Fe^{2.5+}$ iron atoms which share one unpaired electron and a second β pair of two Fe^{3+} atoms—is adequate to describe our results. The **A** and **B** tensors of Table II correspond to the iron atoms of the α pair and the **C** and **D** tensors to the iron atoms of the β pair.

However, comparison of the results in Table II with the previous ones in Table III shows small differences; our isotropic hyperfine values are somewhat greater for the A and B atoms and somewhat smaller for the C and D atoms. But the new result is that, in each α and β pair, *the iron atoms are inequivalent* as indicated by their isotropic as well as their anisotropic hyperfine values. This result is not surprising if we recall the higher resolution attained in our measurements compared with the one characteristic of Mössbauer studies, as discussed above. In fact, this result must reflect the inequivalence of the iron atom environments in the $[Fe_4S_4]^{3+}$ clusters. Even if we consider the primitive $[Fe_4S_4]^{2+}$ cubanes, their reported D_{2d} symmetry is, in fact, only approximate and thus the local environments of the four iron atoms are not completely equivalent.[12] This can be seen in particular if we consider the angles between the external Fe–S bonds (directed toward the benzyl groups) and the Fe–S bonds in the cubane which are different by several degrees and differ for each iron atom as reported in Table IV of ref 12. We shall see later that some other factors may also play a role in explaining this inequivalence.

Next, we must analyze the completely new results, i.e., the principal directions of the four different ^{57}Fe hyperfine tensors of Table II. As is usual in this kind of study, the discussion must be undertaken with reference to the geometry of the primitive $[Fe_4S_4]^{2+}$ cubanes obtained from the X-ray study at room temperature[12] since we do not know the exact geometry of the $[Fe_4S_4]^{3+}$ cluster at the temperature of these experiments. The principal directions of the **A**, **B**, **C**, and **D** tensors have been

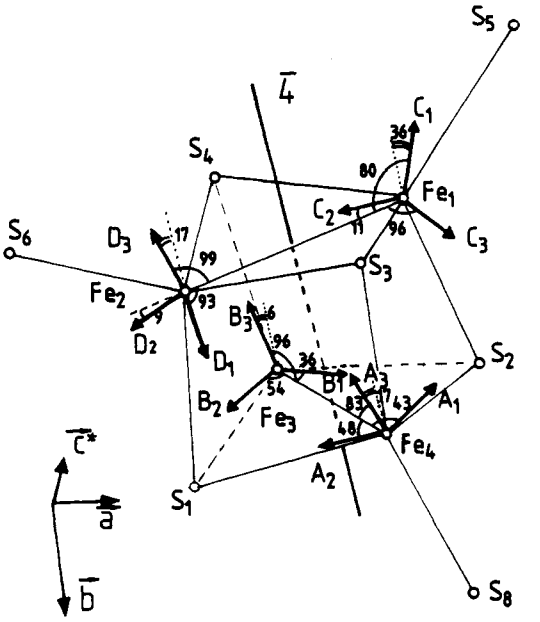

Figure 4. Approximate orientations of the four **A**, **B**, **C**, **D** ^{57}Fe hyperfine tensors with respect to the $(Fe_4S_4)^{2+}$ cubane geometry deduced from ref 12. All the principal axes are labeled following the order of decreasing strengths of the absolute magnitude of the principal values of the tensors, in agreement with their values given in Tables I and II.

systematically compared with all the possible bond directions between each Fe atom and all the other Fe and S atoms (in each of the two magnetically inequivalent cubanes contained in the unit cell), looking for the closest correlation between these principal directions and bond directions. This analysis again highlights the major role played by the two $\overrightarrow{Fe_1Fe_2}$, $\overrightarrow{Fe_3Fe_4}$ directions. The result of this comparison is summarized schematically in Figure 4 where the labeling of the iron atoms follows that used in Figure 2 of ref 12.

We find that, effectively, the principal directions of the **A** and **B** tensors, as well as those of the **C** and **D** tensors, have a peculiar relation (different in the two cases) with these directions. Such a correlation (already observed with the **g** tensor) supports the assignment of the **A** and **B** tensors to the pair of iron atoms labeled 3 and 4 in the X-ray structure[12] and the assignment of the **C** and **D** tensors to those labeled 1 and 2. However, as we have no way to distinguish individually each iron atom, since we refer only to the directions of the iron–iron bonds, we cannot attribute each tensor individually to a defined iron atom within a given pair.

Let us first examine more closely the **A** and **B** tensors of the mixed-valence pair of iron atoms. Evidently, there is not symmetry element which relates these tensors, but we can see in Figure 4 that they are nearly symmetrical with respect to the plane passing by the two iron atoms Fe_1, Fe_2 and perpendicular to the $\overrightarrow{Fe_3Fe_4}$ direction. Thus, the principal axes of the **A** and **B** tensors roughly point toward the sulfur atoms. This result is rather unexpected at first view since recent theoretical models,[17] calculated in D_{2d} symmetry for the cluster structure and in C_{2v} symmetry for the electronic distribution (i.e., in a broken symmetry description), predicted that the last occuppied level of the $[Fe_4S_4]^{3+}$ cluster is essentially built from $d_{x^2-y^2}$ orbitals of the two iron atoms of the mixed-valence pair (where z is parallel to the $\bar{4}$ axis and x and y are parallel to the $\overrightarrow{Fe_1Fe_2}$ and $\overrightarrow{Fe_3Fe_4}$ directions).

Another difficulty appears when we compare the two **C** and **D** tensors of the ferric pair. They are also not simply related and they cannot be associated by an approximate mirror plane symmetry as for the **A** and **B** tensors. Indeed, if they share the same direction (i.e., the Fe_1–Fe_2 bond for their two intermediate principal values), by contrast the greatest hyperfine value of one

(17) Noodleman, L., to be published.

of these tensors corresponds to within 20° with the minimum value of the other, and conversely.

These last two facts concerning the **A** and **B** tensors, on the one hand, and the **C** and **D** tensors, on the other hand, are rather puzzling and we will come back to this point. But, first, we want to point out that the good correspondence observed between certain directions of the tensors and the iron–iron directions is proof that the $[Fe_4S_4]^{3+}$ species created by ionization with the γ-rays in the crystal has not gone through important structural modifications compared with the primitive $[Fe_4S_4]^{2+}$ cubane. Similar conclusions are generally reached in the case of radicals or ionized species created by γ-irradiation in molecular and ionic molecular crystals.

The absence of overall symmetry observed for the $[Fe_4S_4]^{3+}$ center studied here deserves some more comments. As noted above, the primitive $[Fe_4S_4]^{2+}$ cubane in this crystal has not exact but only approximate D_{2d} symmetry.[12] Moreover, upon loss of the electron the two iron pairs α and β become different; there is no reason to suppose that the two Fe_1–Fe_2 and Fe_3–Fe_4 bond distances now remain the same. Thus, the approximate symmetry expected for the $[Fe_4S_4]^{3+}$ cubane is at most C_{2v}. But, since the experimental data show that it is lower, other factors must be considered.

In this respect, we must emphasize that this species corresponds (like all the other species, shown in Figure 1a) to an extra charge trapped on a particular cubane and stable at room temperature after irradiation. The possibility that this trapping may occur in the vicinity of preexisting crystal defects (dislocations, ...), which induce strain fields, cannot be excluded. In such a case, the low symmetry observed would be due to this extrinsic factor. But, there is another mechanism which surely must be considered. The change in the electronic charge occurring at the creation of each $(Fe_4S_4)^{3+}$ center is certainly accompanied by a *relaxation of atomic positions* in the cubane itself and in the surrounding ligands and also by a displacement of the $(NEt_4)^+$ counterions. It is possible that a new nuclear configuration of lowest energy occurs when the extra charge is trapped. This is a *self-trapping mechanism*, in which the atomic displacements are probably small, and which may manifest its effects essentially as a symmetry decrease. But we are not sure that such a process would be sufficient to explain completely our results and, in particular, the observed twist between the principal axes of the two tensors **C** and **D**. We think that, in fact, this point will need further investigation.

V. Conclusion

The $[Fe_4S_4]^{3+}$ state of a four iron–four sulfur cubane has been studied with much higher accuracy than has been previously possible. The complete results obtained here for this paramagnetic state include two sets of data.

(i) The principal values of the **g** and hyperfine tensors have been obtained. The latter, due to the higher precision attained, indicate small inequivalences between iron atoms in the two pairs. However, they agree remarkably well with the previous results, thus establishing completely the validity of our approach and corroborating the model proposed previously.[3c,9,10]

(ii) The principal directions of the ^{57}Fe hyperfine tensors have been determined. This constitutes new results; however, they cannot receive an immediate and satisfactory interpretation. Attempts to refer these results to structures known in synthetic cubanes are not valid for our problem.[18] But we think that, on the contrary, *our results reflect situations very reminiscent of those found in HP ferredoxin proteins*. In effect, the "aperiodic" structure of proteins and the corresponding diversity of amino acid residues composing the environment of each iron atom force us to consider that we cannot have any symmetry at the cubane site. Moreover, upon oxidation from the $(Fe_4S_4)^{2+}$ state to the $(Fe_4S_4)^{3+}$ state, qualitatively similar relaxations of atomic positions in the cubane, and also local rearrangements in its immediate vicinity like those proposed above, must occur to accommodate the charge change.

In order to be able to interpret the latter results, we believe that it is necessary to accumulate more new data of this kind, with as much resolution and precision as possible. We plane to do this in two different directions.

(1) Figure 1a shows that other varieties of the $[Fe_4S_4]^{3+}$ centers are created by γ-irradiation. We feel that gathering ^{57}Fe hyperfine tensors for these other species and comparing them with those of the center described here would be of great help.

(2) In order to complete the mapping of the spin distribution on the atoms of the cubane, it would also be very interesting to obtain complete hyperfine interaction tensors with sulfur in the same way. However, ^{33}S enrichment is much too expensive so we plan to do this in the homologue ^{77}Se-enriched cubanes. But since substitution of selenium for sulfur must somewhat change the electronic structure of the cluster, we will also need to determine the ^{57}Fe hyperfine tensors in the (natural abundance) selenium cubanes.

Acknowledgment. We thank Laurence Vigne for help in the synthesis procedures, Jocelyne Gloux for information on crystallization of the compound, and Louis Noodleman for stimulating discussions.

Registry No. $(Et_4N)_2[Fe_4S_4(SCH_2Ph)_4]$, 52523-51-0; $[Fe_4S_4]^{3+}$, 116564-15-9.

(18) In the past, comparisons of geometries based on X-ray studies of synthetic cubanes between their $(Fe_4S_4)^{2+}$ and $(Fe_4S_4)^+$ states have suggested a compressed-elongated change of the cubane structure under reduction[19]. For the $(Fe_4S_4)^{3+}$ state, much less is known. In the only synthetic complex prepared in this redox state, O'Sullivan and Millar[10a] have reported Fe–S distances slightly shorter than those found in other complexes in their $(Fe_4S_4)^{2+}$ state. This indicates a tendency of strenghtening of these bonds favored by electron loss. In fact, the complete X-ray structure is not known and only the average of iron–iron distances is given. But we want to point out that, even if it were available, it would not give the right element of comparison with the problem posed by our experimental results. In effect, the comparison of the geometrical structures of a defined liganded cubane in two different crystals corresponding to their monocationic and dicationic $(NEt_4)^+$ salts is a rather different problem because *their charges are compensated in each structure by a different number of counterions* giving rise to different environments of the cubane in the two cases.

(19) Laskowski, E. J.; Reynolds, J. G.; Frankel, R. B.; Foner, S.; Papaefthymiou, G. C.; Holm, R. H. *J. Am. Chem. Soc.* **1979**, *101*, 6562.